Journal of Applied Physics

Comparison of enhanced second harmonic generation in pyramid-like in-plane MoS_2 flakes to vertically aligned MoS_2 flakes

Cite as: J. Appl. Phys. **129**, 063106 (2021); https://doi.org/10.1063/5.0035738
Submitted: 31 October 2020 • Accepted: 24 January 2021 • Published Online: 11 February 2021

Abhay V. Agrawal, Robert Lemasters, Chentao Li, et al.

AIP Publishing

Journal of Applied Physics ARTICLE scitation.org/journal/jap

Comparison of enhanced second harmonic generation in pyramid-like in-plane MoS_2 flakes to vertically aligned MoS_2 flakes

Cite as: J. Appl. Phys. **129**, 063106 (2021); doi: 10.1063/5.0035738
Submitted: 31 October 2020 · Accepted: 24 January 2021 ·
Published Online: 11 February 2021

View Online Export Citation CrossMark

Abhay V. Agrawal,[1] Robert Lemasters,[2] Chentao Li,[2] Ali Mojibpour,[3] Palash Bharadwaj,[3] Hayk Harutyunyan,[2,a)] and Mukesh Kumar[1,a)]

AFFILIATIONS

[1]Functional and Renewable Energy Materials Laboratory, Indian Institute of Technology Ropar, Punjab 140001, India
[2]Department of Physics, Emory University, Atlanta, Georgia 30322, USA
[3]Department of Electrical and Computer Engineering, Rice University, Houston, Texas 77005, USA

[a)]**Authors to whom correspondence should be addressed:** hayk.harutyunyan@emory.edu and mkumar@iitrpr.ac.in

ABSTRACT

Here, we report the comparative study of enhanced second harmonic generation using defect engineering in pyramid-like MoS_2 (P-MoS_2) flakes to vertically aligned MoS_2 (VA-MoS_2) flakes. P-MoS_2 and VA-MoS_2 is synthesized via the modified chemical vapor deposition technique. The second harmonic generation measurements on P-MoS_2 and VA-MoS_2 are performed by sweeping the excitation wavelength from 1200 nm to 1310 nm in identical conditions. The P-MoS_2 flakes show a high SHG signal. The high SHG signal in pyramid-like MoS_2 is attributed to the broken inversion symmetry and high thickness of grown MoS_2 flakes. VA-MoS_2 flakes under the identical conditions show a 34% enhanced SHG signal in comparison to P-MoS_2. The midgap states generated due to defects in the form of S vacancies in VA-MoS_2 are responsible for this enhancement. These midgap states confine the photons and result in enhanced SHG properties. Our study will pave a new path to understand the role of 2D material morphology in fabricating versatile optical and photonics devices.

I. INTRODUCTION

Transition metal dichalcogenides (TMDCs) have grabbed potential attraction due to their unique physical, mechanical, and optical properties.[1] MoS_2 belongs to the TMDC family that has intensively become the focus of the research community due to its wide and unique applications in next generation optical and electronic devices.[2–4]

Recently, MoS_2 showed promising applications in the field of photonics.[5–7] A single layer of MoS_2 consists of two sulfur layers with one sandwiched molybdenum layer in between and possesses a direct bandgap of 1.8 eV. MoS_2 based photodetectors, solar cells, gas sensors, and photodiodes have shown favorable fast performance compared to other traditional materials.[5,8–10] Apart from these properties, MoS_2 has potential in the areas of valleytronics, spintronics, and nonlinear optics, especially in second harmonic generation (SHG).[6,11–14] The 2H-bulk MoS_2 exhibits a very small SHG response due to the existing inversion symmetry and belongs to the D^1_{3d} symmetry group.[15] However, monolayer (or odd number layer numbers) MoS_2 belonging to the D^1_{3h} symmetry group has a broken inversion symmetry and shows promising SHG nonlinearities,[16] while the bilayer MoS_2 (even layer number) retains an inversion symmetry with almost vanishing SHG nonlinearities.[14,17,18]

Recent progress in the synthesis and orientation of MoS_2 flakes has opened a new path for exploring the new optical properties of MoS_2 flakes.[19–21] It has been well documented that edges play a vital role in enhancing the optical and electrical properties.[22–26] Yin and his co-workers reported that the SHG response is greatly affected by the edges in comparison to the central part of the MoS_2 flakes due to variations in the electronic structure between the edges and monolayers.[27] However, the micron size of a typical grown in-plane MoS_2 flake limits the non-linear interaction length and diminishes this effect.[28] Thus, further approaches have been required to increase the interaction length to further enhance the SHG properties. There are some other approaches to enhance the interaction length such as formation of hybrid structures, microcavities, and use of plasmonics.[1,13,16,29]

Over the past few years, significant effort has been made to grow large areas of MoS_2 flakes. It has been reported that the edges of 2D materials have a larger number of optically active sites in comparison to pyramid-like 2D materials.[30] There have been several studies which have aimed to increase the exposed edges by synthesizing stacked P-MoS_2 geometries.[31–34] Lin and his co-workers studied the enhanced SHG response in pyramid WS_2 which was attributed to the high number of edges.[30] These P-WS_2 flakes increase the SHG properties. Another approach is to increase the number of edges by synthesizing VA-MoS_2 flakes. VA-MoS_2 flakes have a higher number of exposed edges in comparison to in-plane MoS_2 flakes.[31,35–37] MoS_2 edges have a metallic-like nature, defect states, and strong light–matter interactions.[22] MoS_2 edges have shown promise in the application of developing next-generation devices. Moreover, VA-MoS_2 has demonstrated high quality and scalable properties in developing broadband, fast-response photodetectors, energy storage devices, gas sensors, water disinfection, and catalytic applications.[36,38–41] However, there are a very few reports where these edges are used to study the SHG properties.[42,43] Thus, significant approaches are required to explore the role of edges in the properties of SHG by modifying the structure of the MoS_2 flakes.

Here, we report the comparative study of SHG properties between the VA-MoS_2 flakes and the P-MoS_2 flakes. The VA-MoS_2 flakes are synthesized by our previously reported method.[19] However, to synthesize the P-MoS_2 flakes, the growth time and gas flow rate are further optimized. The second harmonic generation measurements are performed for detection wavelengths of 600 to 655 nm. We find that the SHG signal is enhanced in VA-MoS_2 flakes up to 34% in comparison to P-MoS_2 flakes.

II. EXPERIMENTAL SECTION

A. Growth of VA-MoS_2 flakes

MoO_3 (0.057 mg, 99.97%) and S (0.45 g, 99.98%) powder, provided by Sigma-Aldrich, are used to synthesize the MoS_2 flakes. Initially, the SiO_2/Si (300 nm/250 μm) substrates are sonicated for 20 min in acetone. Following sonication, the substrate is cleaned with a nitrogen gas jet. The clean substrate is put on top of a zirconia boat containing MoO_3 powder. A modified tube-in-tube atmospheric chemical vapor deposition (APCVD) setup is used to grow VA-MoS_2 flakes. The detailed description is given in our previous reports.[19] A small quartz tube is used to synthesize the vertically aligned and pyramid-like MoS_2 flakes. The S powder is placed at the open end of a small tube, while the MoO_3 powder and the substrate are placed at the closed end of a small tube. This arrangement is then placed in a bigger quartz tube. The CVD setup has three zones. The closed end of the tube is put in zone 1 with a temperature of 800 °C, and the open end of the tube is in zone 2 with a growth temperature of 350 °C. The gas flow rate during the whole deposition is fixed at 175 SCCM. The growth time is 30 min. Finally, the system is cooled down ambiently following deposition.

B. Growth of P-MoS_2 flakes

The APCVD setup for the synthesis of P-MoS_2 flakes is the same as for VA-MoS_2 flakes, except for the gas flow rate and growth time. The cleaning process of the substrate, amount, and temperature profile is exactly the same as for VA-MoS_2 flakes. To grow pyramid MoS_2 flakes, the gas flow is initially kept at 175 SCCM, then slowly decreased down to 50 SCCM. The growth time of the synthesis is 5 min. The critical parameter to obtain the P-MoS_2 flakes is to precisely control the sulfurization rate. The P-MoS_2 growth arises due to the screw dislocations generated in the initial stage of the growth.[34] Initially, the gas flow rate is high (175 SCCM). Thus, vaporized sulfur quickly reacts with MoO_3 and produces reduced MoO_{3-x} in a short time.[44,45] Thus, the probability of the formation of new accidental nucleation sites on the grown film surface is very high.[46] Once an accidental plane is grown, it becomes a favorable site for upcoming S and Mo vapors due to the reduced energy barrier.[47] Next, the gas flow rate is slowly decreased to avoid the formation of VA-growth and new nucleation sites. The upcoming atomic species is attached to the already formed MoS_2 planes in the vertical direction and leads to the formation of the P-MoS_2 flakes. The schematic of the CVD setup used to grow vertical P-MoS_2 is shown in Fig. 1(a).

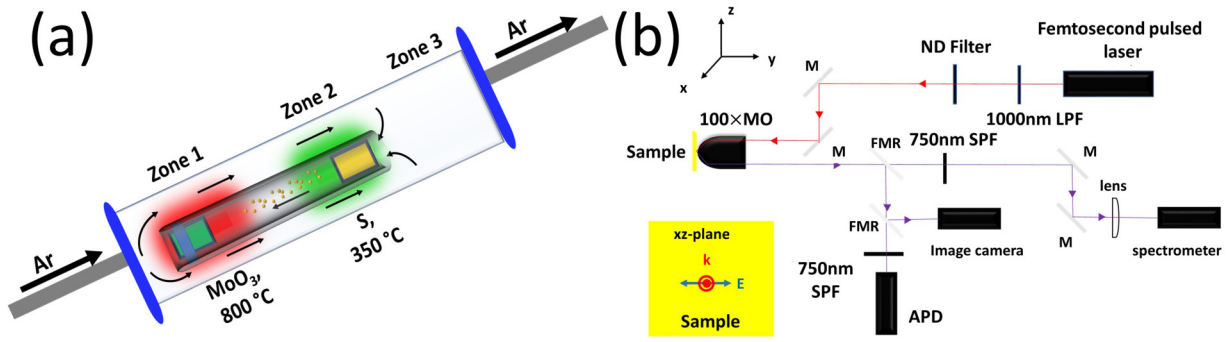

FIG. 1. (a) Schematic of the modified APCVD setup used to grow VA-MoS_2 and P- MoS_2 flakes. S powder was placed at the open end of the small tube, and MoO_3 powder with the substrate was placed at the close end of the small tube. (b) SHG setup schematic used for measurements. The SHG measurements are carried out in the pump in the wavelength range of 1200–1310 nm. A full description is given in the text.

C. Characterization

Field emission scanning electron microscopy (FE-SEM) is performed by using the JEOL 7600F system with an accelerating voltage of 3 kV. Raman measurements were performed through a HORIBA setup equipped with a 532 nm continuous wave laser and a 100× magnification objective lens. The spot size of the laser is 0.5 μm. The surface topography of P-MoS_2 samples is carried out using atomic force microscopy (AFM) in a tapping mode using a Bruker make scanning probe microscope.

To perform the SHG measurements, a Chameleon Ultra II Ti: sapphire femtosecond laser is used as the excitation source. The repetition rate is 80 MHz, and the pump wavelength continuously varies from 1200 nm to 1310 nm. The measurements are performed in a reflection geometry with the same 100 × 0.9 NA objective being used for excitation as well as collection. Scanning maps of the surface of the sample are obtained by controlling the movement of the piezo stage and monitoring the SHG signals with an avalanche photodiode (APD). SHG spectra are measured by a spectrometer, in which a CCD array detects signals ranging from 400 nm to 1000 nm. The full optical setup is shown in detail in Fig. 1(b).

III. RESULTS AND DISCUSSION

The morphology and surface topography of both P-MoS_2 and VA-MoS_2 flakes are characterized by FE-SEM and AFM.

Figure 2(a) shows the low magnification FE-SEM image of the grown P-MoS_2 flakes. The growth of P-MoS_2 flakes is highly uniform as can be seen from the surface morphology. High magnification FE-SEM of the pyramid MoS_2 is shown in Fig. 2(b). The surface topography is further analyzed by the AFM. It is seen that the density of the P-MoS_2 flakes is so high that they start to agglomerate with each other and forms combined P-MoS_2 flakes. The line profile study of an individual pyramid is shown in Fig. 2(d). The height of the pyramid is varied up to 14 nm, corresponding to 20 layers. The average size of P-MoS_2 flakes is 400 to 500 nm. The schematic of P-MoS_2 is shown in Fig. 2(d).

The low magnification FE-SEM image of VA-MoS_2 flakes is shown in Fig. 3(a). The VA-MoS_2 flakes have very uniform growth and are highly dense with a large coverage area on the SiO_2/Si substrate. The high magnification image of VA-MoS_2 flakes is shown in Fig. 3(b). The height of the VA-MoS_2 flakes is between 200 and 500 nm.

Moreover, the vibrational properties of both structures are characterized using Raman spectroscopy as shown in Fig. 3(c). MoS_2 flakes have two well-known Raman vibrations due to the vibration of S and Mo atoms.[19,38,48] The E^1_{2g} and A_{1g} peaks are located at 382.06 (379.94) and 405.30 (406.69) cm^{-1} for pyramid-like (vertically aligned) structures. E^1_{2g} and A_{1g} correspond to in-plane and out-of-plane vibrations, respectively. E^1_{2g} arises due to vibrations of Mo and S atoms, while A_{1g} arises due to out-of-plane vibrations of S atoms.[48] Thus, the peak intensity ratio of E^1_{2g} and A_{1g} can be used to determine the orientation of MoS_2 flakes. The peak ratio of P-MoS_2 flakes is 0.59, while of VA-MoS_2, it is 0.42. The peak ratio clearly demonstrates the existing geometries of P-MoS_2 consisting of in-plane flakes, while the VA-MoS_2 flakes have edges.[19] This confirms that the Raman signals are coming from the exposed edges in the case of VA-MoS_2 flakes and from the terrace of MoS_2 in P-MoS_2. The difference between these two peaks is 24 to 25 cm^{-1}, confirming the few layers of flakes in P-MoS_2 and VA-MoS_2. It is observed that

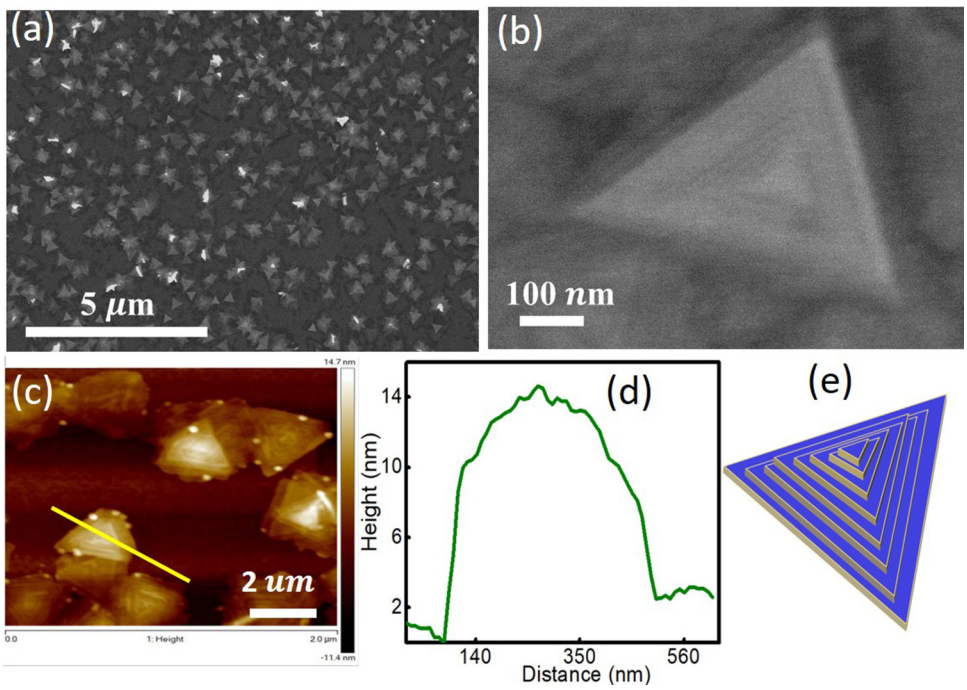

FIG. 2. (a) The low magnification FE-SEM image of P-MoS_2. The synthesized P-MoS_2 flakes uniformly covered the whole substrate. (b) High magnification FE-SEM image of single P-MoS_2, confirming the pyramid-like stacked nature of P-MoS_2. (c) AFM surface topography of highly dense P-MoS_2. In some regions, P-MoS_2 agglomerates with each other. (d) The height profile across an individual pyramid MoS_2 flakes. Most of the pyramids have an average height of 14 nm with a size of 400–500 nm. (e) Schematic of P-MoS_2.

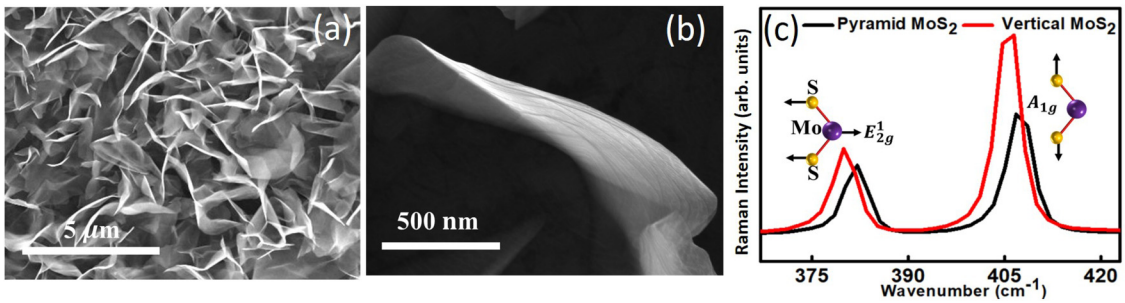

FIG. 3. (a) Low magnification FE-SEM image of highly uniform VA-MoS_2 flakes. The VA-MoS_2 flakes are uniformly grown over the entire substrate and are well connected with each other. (b) High magnification FE-SEM image of a vertical aligned layer of VA-MoS_2 flakes. (c) Raman spectra obtained from VA-MoS_2 and P-MoS_2 flakes. The VA-MoS_2 flakes have a smaller E^1_{2g}/A_{1g} ratio in comparison to P-MoS_2 flakes. The intensity ratio further confirming the orientation of the flakes.

both peak positions in the case of P-MoS_2 are red-shifted in comparison to the VA-MoS_2 flakes. This may be due to the higher number of interlayer coupling between the layers of P-MoS_2 flakes.[34,48]

Figures 4(a) and 4(b) show the optical image and APD scans of the P-MoS_2. The optical image further verifies the uniformly distributed P-MoS_2 flakes. After the linear resonance, a MoS_2 flake has been identified by photoluminescence measurements. The wavelength-dependent SHG measurements are performed by sweeping the excitation wavelength from 1200 nm to 1310 nm, and the results are shown in Fig. 4(c). A very small beam diameter

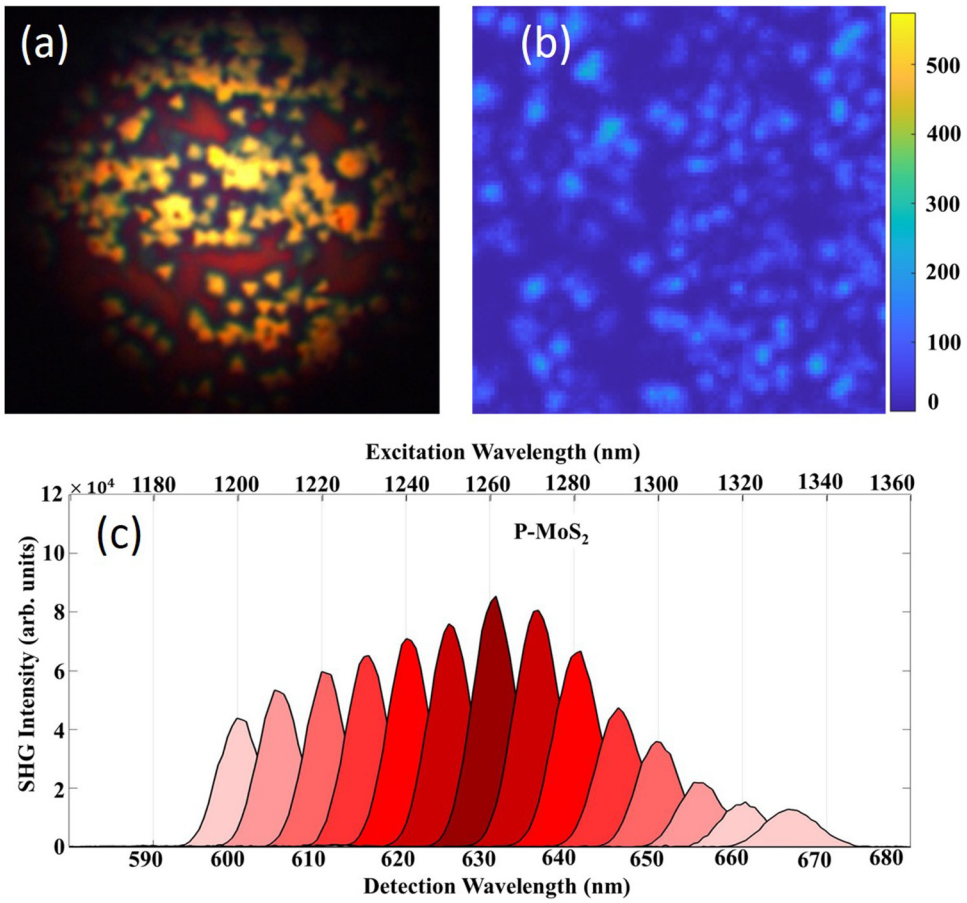

FIG. 4. (a) Optical scan of the P-MoS_2 flakes, further confirming the uniformity with interconnected nature over the substrate. (b) APD scan for an excitation wavelength of 1300 nm. The size of the image is 20 μm^2. (c) SHG spectra measured at different excitation wavelengths for P-MoS_2 flakes. The data are normalized by the respective excitation power. The color code is just a visual guide.

(around 2 mm) is used in order to get an approximately normal incidence. It is observed that incident light radiated from the center of P-MoS_2, signifying efficient constructive generation of the SHG signal. The P-MoS_2 flakes give the strongest SHG signal at around 620 nm. This peak corresponds to the B exciton mode of the monolayer MoS_2, ensuring that most of the SHG signals come from the flakes themselves.[49,50] It has been reported that in-plane MoS_2 can have two types of stacking orders.[51–53] In one order, the Mo–S bond direction of the central layer can be opposite to the Mo–S bond directions of the neighboring layers. Such MoS_2 structures belong to D^1_{3d} groups and have an inversion symmetry with weak SHG signals. In the other stacking order, the Mo–S bond direction of the central layer is in the same direction as the Mo–S bond directions of neighboring layers. Such structures have a broken inversion symmetry and belong to the D^1_{3h} group with strong SHG signals. Our results indicated that our grown P-MoS_2 structures have the broken inversion symmetry and, consequently, exhibit very strong SHG signals. Another important feature of our grown P-MoS_2 flakes is the high thickness. P-MoS_2 has a high number of layers that increases the thickness of the MoS_2 flakes. The large thickness of the MoS_2 flakes permits an enhanced light–matter sub-atomic interaction length, which leads to high SHG signals for all wavelengths that are absent in the case of monolayer MoS_2 flakes.[30,54] It is worth to note that synthesized MoS_2 pyramids do not have the same size. Some pyramids are of smaller and some are larger in size. Shearer *et al.* investigated the role of pyramid sizes in generating SHG signals.[55] The authors synthesized the stacked pyramids of WSe_2 triangles of the same height but with of different sizes of 5.4, 4.5, 4.2, and 4 μm. They observed that the SHG signal intensity increased as the size of the pyramid WSe_2 flakes increased. The high SHG intensity was due to enhanced constructive interference by the larger size pyramid structures. Similarly, we believe in our case that the SHG intensity will also increase with the larger size of the grown MoS_2 pyramids.

Finally, SHG measurements are performed on the highly uniform VA-MoS_2 flakes. Figures 5(a) and 5(b) show the optical image and APD scans of the VA-flakes. Again, all measurements are performed under the identical conditions as for P-MoS_2 flakes. It is observed that, for both the in-plane and VA-MoS_2 flakes, the strongest SHG signal is seen at around 620 nm. It has been observed that SHG intensity values for the wavelength from 600 to 640 nm are similar. However, the overall trend shows a clear maximum at the 620 nm wavelength. The most intense peak is at

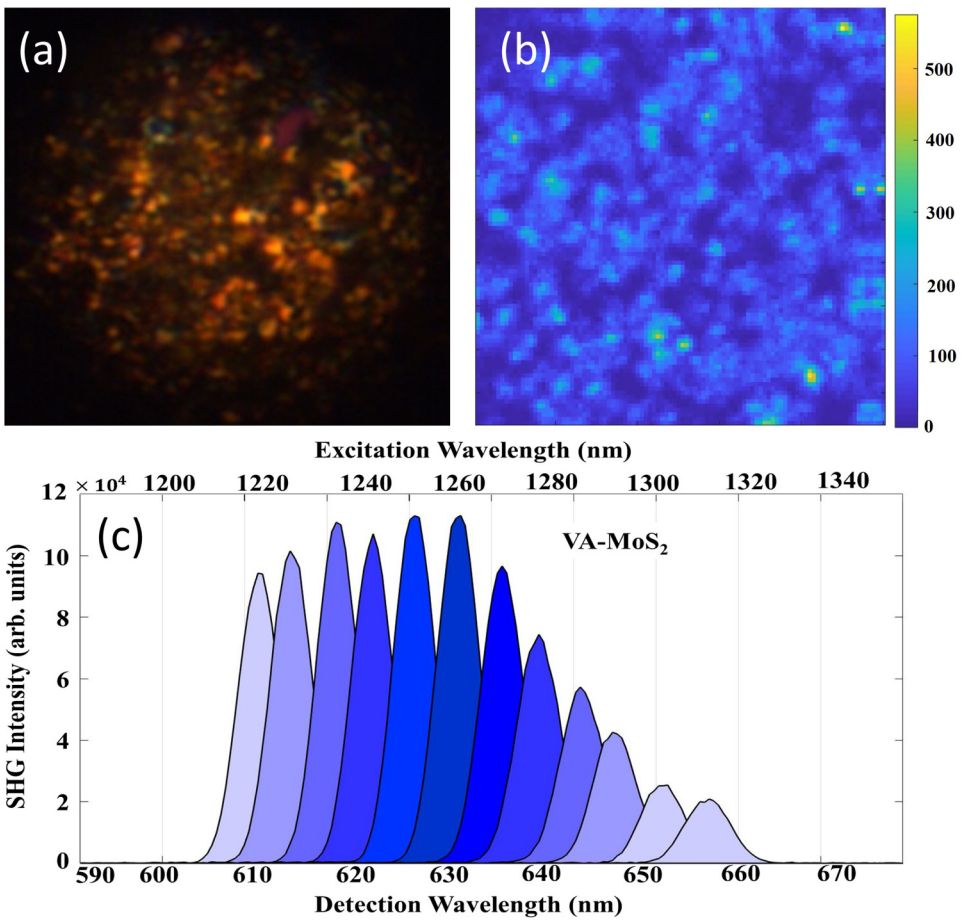

FIG. 5. (a) Optical image of the VA-MoS_2 flakes. (b) APD scan for an excitation wavelength of 1300 nm. The size of the image is20 μm^2. (c) SHG spectra measured at different excitation wavelengths for VA-MoS_2 flakes. The data are normalized by the respective excitation power. The color code is just a visual guide.

620 nm corresponding to the B excitation mode of MoS_2 photoluminescence, while the other peaks are due to the presence of midgap states in both structures. These midgap states provide better photon confinement for SHG enhancement.

More importantly, having normalized the excitation with the respective power, we find that the average SHG signal from the VA-samples is larger than that of P-sample ones. The peak signals of VA-MoS_2 flakes are up to 110 000 counts at 620 nm, while the P-flakes only generate up to 82 000 counts, as shown in Figs. 4(c) and 5(c). Therefore, an enhancement of around 34% can be achieved by modifying the MoS_2 structure to an edge-enriched one. The nonlinear efficiencies for the two materials are calculated and given in the supplementary material. It is worth noting that, in the SHG measurement, a linearly polarized TE mode excitation beam is used. In order to compensate for the potential inhomogeneity of SHG signals caused by the polarization, the most optically active areas among all the MoS_2 flakes as revealed in the APD scanning maps are chosen to determine the peak signals. Due to the random displacement of MoS_2 flakes on the substrates as shown in Fig. 2(a), the linearly polarized excitation could statistically still give reliable SHG results without affecting the comparability between Figs. 4(c) and 5(c).

It can be seen that edges play a vital role in enhancing the SHG intensity. In our report, the high SHG signal of the P-MoS_2 is ascribed to the presence of a large number of edges and to the constructive interferences between the stacked planes in MoS_2 pyramids. The planes of the synthesized pyramids shrink with their height and so we have the maximum number of exposed MoS_2 edges in pyramid-like structures. The high SHG signal can be considered as the effect of the number of enhanced edges as well as the constructive interference taking place between them. It has been reported that the SHG signal is enhanced along the edges in comparison with the terrace sites of MoS_2, which may be due to the presence of additionally occupied edge states.[27] Also, each stacked layer of the MoS_2 pyramid offers constructive interference with each neighboring layer. The single layer of MoS_2 has the broken inversion symmetry, and it has the stacking in the AbA manner. Generally, the second layer has the stacking like in the BaB manner. So, synthesizing multilayer MoS_2 flakes is not good as the destructive interference takes place with the multilayer MoS_2 film. During the growth of pyramid MoS_2 flakes, due to screw dislocations, the upper layer grows on the lower layer in such a way that they both stacked in the same manner, and the second upper layer also has the stacking in the AbA manner. Thus, the layers have constructive interferences with each neighboring layer and SHG signal enhanced. The similar behavior is also observed in various other reports.[30,34,44,55]

However, in the case of the VA-MoS_2 flakes, defects play the role for further enhancement. In our previous study, we observed that edges have defects in the form of dangling bonds, S vacancies, and adsorbed oxygens.[38] During the CVD growth of these unique structures, nucleation sites, coalescence, and stress and strain energy are responsible for the S vacancy generation. In a recent report by Zhou and his co-workers, they studied the intrinsic structural defects in the monolayer MoS_2.[56] The most possible types of defects are a mono-sulfur vacancy, di-sulfur vacancy, single Mo atom vacancy, and Mo atom with three sulfur, three di-sulfur pairs.[56] Also, the energy required to remove an S atom is 6.1 eV, while for Mo atoms, it is 13.9 eV.[57] The S vacancies create midgap states in the MoS_2 bandgap, and SHG signals are strongly dependent on the density of S vacancies. Thus, S vacancy generation is more probable and beneficial for SHG measurements. It is worth mentioning that we achieve the SHG signal for the 1200 to 1310 nm excitation wavelength range. The most intense peak is at 620 nm corresponding to the B excitation mode of MoS_2 photoluminescence, while the other peaks are due to the presence of midgap states in both structures.[50] These midgap states provide better photon confinement for SHG enhancement.[58] We believe that our study will pave a new path to understand the role of 2D material morphology in fabricating versatile optical and photonics devices.

IV. CONCLUSION

Here, we synthesize P-MoS_2 and VA-MoS_2 through the modified CVD technique. FE-SEM measurements confirm the surface morphology of the highly uniform VA-MoS_2 and P-MoS_2 flakes. The surface topography analyzed by AFM measurements reveal that P-MoS_2 have a height of ~14 nm corresponding to 20 stacked monolayers with an area of 400 to 500 nm. The detailed SHG performance shows that VA-MoS_2 flakes have a 34% higher SHG signal intensity as compared to P-MoS_2 flakes. The high SHG signal is due to midgap states that arise due to defects present at the edges, which enhance the SHG signal intensity in VA-MoS_2 flakes.

SUPPLEMENTARY MATERIAL

See the supplementary material for the calculated conversion efficiency of P-MoS_2 and VA-MoS_2 for both structures.

ACKNOWLEDGMENTS

A.V.A. and M.K. acknowledge financial support from the Department of Atomic Energy (DAE) under Project No. 34/20/09/2015/BRNS and also the Department of Physics, IIT Ropar, for providing experimental facilities. R.L., C.L., and H.H. acknowledge the National Science Foundation (NSF) (No. EFMA-1741691).

DATA AVAILABILITY

The data that support the findings of this study are available from the corresponding authors upon reasonable request.

REFERENCES

[1]H. Chen, V. Corboliou, A. S. Solntsev, D.-Y. Choi, M. A. Vincenti, D. de Ceglia, C. de Angelis, Y. Lu, and D. N. Neshev, Light Sci. Appl. **6**, e17060 (2017).
[2]M. Chhowalla, H. S. Shin, G. Eda, L. J. Li, K. P. Loh, and H. Zhang, Nat. Chem. **5**, 263 (2013).
[3]J. K. Day, M.-H. Chung, Y.-H. Lee, and V. M. Menon, Opt. Mater. Express **6**, 2360 (2016).
[4]A. V. Agrawal, N. Kumar, and M. Kumar, Nano-Micro Lett. **13**, 38 (2021).
[5]O. Lopez-Sanchez, D. Lembke, M. Kayci, A. Radenovic, and A. Kis, Nat. Nanotechnol. **8**, 497 (2013).
[6]X. Yin, Z. Ye, D. A. Chenet, Y. Ye, K. O'Brien, J. C. Hone, and X. Zhang, Science **344**, 488 (2014).
[7]Q. Liu, B. Cook, M. Gong, Y. Gong, D. Ewing, M. Casper, A. Stramel, and J. Wu, ACS Appl. Mater. Interfaces **9**, 12728 (2017).

[8]V. Dhyani and S. Das, Sci. Rep. **7**, 44243 (2017).
[9]M. Bernardi, M. Palummo, and J. C. Grossman, ACS Nano **6**, 10082 (2012).
[10]X. Geng, Y. Guo, D. Li, W. Li, C. Zhu, X. Wei, M. Chen, S. Gao, S. Qiu, and Y. Gong, Sci. Rep. **3**, 1134 (2013).
[11]K.-I. Lin, Y.-H. Ho, S.-B. Liu, J.-J. Ciou, B.-T. Huang, C. Chen, H.-C. Chang, C.-L. Tu, and C.-H. Chen, Nano Lett. **18**, 793 (2018).
[12]M. L. Trolle, Y.-C. Tsao, K. Pedersen, and T. G. Pedersen, Phys. Rev. B **92**, 161409 (2015).
[13]J. Zeng, M. Yuan, W. Yuan, Q. Dai, H. Fan, S. Lan, and S. Tie, Nanoscale **7**, 13547 (2015).
[14]L. M. Malard, T. V. Alencar, A. P. M. Barboza, K. F. Mak, and A. M. De Paula, Phys. Rev. B **87**, 201401 (2013).
[15]G. A. Wagoner, P. D. Persans, E. A. Van Wagenen, and G. M. Korenowski, J. Opt. Soc. Am. B **15**, 1017 (1998).
[16]N. Kumar, S. Najmaei, Q. Cui, F. Ceballos, P. M. Ajayan, J. Lou, and H. Zhao, Phys. Rev. B **87**, 161403 (2013).
[17]Y. Li, Y. Rao, K. F. Mak, Y. You, S. Wang, C. R. Dean, and T. F. Heinz, Nano Lett. **13**, 3329 (2013).
[18]H. Zeng, G.-B. Liu, J. Dai, Y. Yan, B. Zhu, R. He, L. Xie, S. Xu, X. Chen, and W. Yao, Sci. Rep. **3**, 1608 (2013).
[19]A. V. Agrawal, N. Kumar, S. Venkatesan, A. Zakhidov, C. Manspeaker, Z. Zhu, F. C. Robles Hernandez, J. Bao, and M. Kumar, ACS Appl. Nano Mater. **1**, 2356 (2018).
[20]D. Kong, H. Wang, J. J. Cha, M. Pasta, K. J. Koski, J. Yao, and Y. Cui, Nano Lett. **13**, 1341 (2013).
[21]Y. Jung, J. Shen, Y. Liu, J. M. Woods, Y. Sun, and J. J. Cha, Nano Lett. **14**, 6842 (2014).
[22]M. V. Bollinger, J. V. Lauritsen, K. W. Jacobsen, J. K. Nørskov, S. Helveg, and F. Besenbacher, Phys. Rev. Lett. **87**, 196803 (2001).
[23]T. F. Jaramillo, K. P. Jørgensen, J. Bonde, J. H. Nielsen, S. Horch, and I. Chorkendorff, Science **317**, 100 (2007).
[24]H. Wang, Q. Zhang, H. Yao, Z. Liang, H. W. Lee, P. C. Hsu, G. Zheng, and Y. Cui, Nano Lett. **14**, 7138 (2014).
[25]M. Kumar, A. V. Agrawal, M. Moradi, and R. Yousefi, in *Nanomaterials for Air Remediation*, edited by A. Abdeltif, A. A. Assadi, P. Nguyen-Tri, T. A. Nguyen, and S. Rtimi (Elsevier, 2020), p. 107.
[26]A. V. Agrawal, R. Kumar, G. Yang, J. Bao, M. Kumar, and M. Kumar, Int. J. Hydrogen Energy **45**, 9268 (2020).
[27]X. Yin, Z. Ye, D. A. Chenet, Y. Ye, K. O'Brien, J. C. Hone, and X. Zhang, Science **344**, 488 (2014).
[28]H. Hora, "Y. R. Shen: The principle of nonlinear optics," in *Laser and Particle Beams* (John Wiley & Sons, New York, 1984), p. 576.
[29]S. Shree, I. Paradisanos, X. Marie, C. Robert, and B. Urbaszek, Nat. Rev. Phys. **3**, 39–54 (2020).
[30]X. Lin, Y. Liu, K. Wang, C. Wei, W. Zhang, Y. Yan, Y. J. Li, J. Yao, and Y. S. Zhao, ACS Nano **12**, 689 (2018).
[31]Q. Zhou, S. Su, P. Cheng, X. Hu, X. Gao, Z. Zhang, and J.-M. Liu, J. Mater. Chem. C **8**, 3017 (2020).
[32]Q. Zhou, S. Su, P. Cheng, X. Hu, M. Zeng, X. Gao, Z. Zhang, and J.-M. Liu, Nanoscale **10**, 11578 (2018).
[33]A. Mills, Y. Yu, C. Chen, B. Huang, L. Cao, and C. Tao, Appl. Phys. Lett. **108**, 081601 (2016).
[34]L. Zhang, K. Liu, A. B. Wong, J. Kim, X. Hong, C. Liu, T. Cao, S. G. Louie, F. Wang, and P. Yang, Nano Lett. **14**, 6418 (2014).
[35]A. V. Agrawal, R. Kumar, S. Venkatesan, A. Zakhidov, G. Yang, J. Bao, M. Kumar, and M. Kumar, ACS Sens. **3**, 998 (2018).
[36]A. V. Agrawal, K. Kaur, and M. Kumar, Appl. Surf. Sci. **514**, 145901 (2020).
[37]S. Zhang, J. Liu, K. H. Ruiz, R. Tu, M. Yang, Q. Li, J. Shi, H. Li, L. Zhang, and T. Goto, Materials **11**, 631 (2018).
[38]A. V. Agrawal, R. Kumar, S. Venkatesan, A. Zakhidov, Z. Zhu, J. Bao, M. Kumar, and M. Kumar, Appl. Phys. Lett. **111**, 093102 (2017).
[39]A. V. Agrawal and M. Kumar, Mater. Res. Express **6**, 115011 (2019).
[40]C. Liu, D. Kong, P.-C. Hsu, H. Yuan, H.-W. Lee, Y. Liu, H. Wang, S. Wang, K. Yan, D. Lin, P. A. Maraccini, K. M. Parker, A. B. Boehm, and Y. Cui, Nat. Nanotechnol. **11**, 1098 (2016).
[41]M.-L. Tsai, S.-H. Su, J.-K. Chang, D.-S. Tsai, C.-H. Chen, C.-I. Wu, L.-J. Li, L.-J. Chen, and J.-H. He, ACS Nano **8**, 8317 (2014).
[42]M. Bolhuis, J. Hernandez-Rueda, S. E. van Heijst, M. Tinoco Rivas, L. Kuipers, and S. Conesa-Boj, Nanoscale **12**, 10491 (2020).
[43]R. Wei, X. Tian, Z. Hu, H. Zhang, T. Qiao, X. He, Q. Chen, Z. Chen, and J. Qiu, Opt. Express **24**, 25337 (2016).
[44]X. Fan, Y. Zhao, W. Zheng, H. Li, X. Wu, X. Hu, X. Zhang, X. Zhu, Q. Zhang, X. Wang, B. Yang, J. Chen, S. Jin, and A. Pan, Nano Lett. **18**, 3885 (2018).
[45]I. V. Markov, *Crystal Growth for Beginners: Fundamentals of Nucleation, Crystal Growth and Epitaxy* (World Scientific, 2016).
[46]A. Zhuang, J.-J. Li, Y.-C. Wang, X. Wen, Y. Lin, B. Xiang, X. Wang, and J. Zeng, Angew. Chem., Int. Ed. **53**, 6425 (2014).
[47]P. Kumar and B. Viswanath, Cryst. Growth Des. **16**, 7145 (2016).
[48]C. Lee, H. Yan, L. E. Brus, T. F. Heinz, J. Hone, and S. Ryu, ACS Nano **4**, 2695 (2010).
[49]K. F. Mak, C. Lee, J. Hone, J. Shan, and T. F. Heinz, Phys. Rev. Lett. **105**, 136805 (2010).
[50]A. Splendiani, L. Sun, Y. Zhang, T. Li, J. Kim, C.-Y. Chim, G. Galli, and F. Wang, Nano Lett. **10**, 1271 (2010).
[51]X. Lin, Y. Liu, K. Wang, X. Liu, Y. Yan, Y. J. Li, J. Yao, and Y. S. Zhao, Research **2018**, 4164029.
[52]X. Fan, Z. Ji, R. Fei, W. Zheng, W. Liu, X. Zhu, S. Chen, L. Yang, H. Liu, A. Pan, and R. Agarwal, Nano Lett. **20**, 2667 (2020).
[53]X. Wen, Z. Gong, and D. Li, InfoMat **1**, 317 (2019).
[54]X. Fan, Y. Jiang, X. Zhuang, H. Liu, T. Xu, W. Zheng, P. Fan, H. Li, X. Wu, X. Zhu, Q. Zhang, H. Zhou, W. Hu, X. Wang, L. Sun, X. Duan, and A. Pan, ACS Nano **11**, 4892 (2017).
[55]M. J. Shearer, L. Samad, Y. Zhang, Y. Zhao, A. Puretzky, K. W. Eliceiri, J. C. Wright, R. J. Hamers, and S. Jin, J. Am. Chem. Soc. **139**, 3496 (2017).
[56]W. Zhou, X. Zou, S. Najmaei, Z. Liu, Y. Shi, J. Kong, J. Lou, P. M. Ajayan, B. I. Yakobson, and J.-C. Idrobo, Nano Lett. **13**, 2615 (2013).
[57]X. Liu, T. Xu, X. Wu, Z. Zhang, J. Yu, H. Qiu, J. H. Hong, C. H. Jin, J. X. Li, X. R. Wang, L. T. Sun, and W. Guo, Nat. Commun. **4**, 1776 (2013).
[58]H. G. Rosa, L. Junpeng, L. C. Gomes, M. J. L. F. Rodrigues, S. C. Haur, and J. C. V. Gomes, Adv. Opt. Mater. **6**, 1701327 (2018).